8-14-2017

Amorphous Boron Nanorod as an Anode Material for Lithium-Ion Batteries at Room Temperature

Changjian Deng
Boise State University

Miu Lun Lau
Boise State University

Riley Parrish
Boise State University

Kassiopeia A. Smith
Boise State University

Hui Xiong
Boise State University

View Article Online
DOI: 10.1039/C7NR03017G

Nanoscale

ARTICLE

Amorphous Boron Nanorod as Anode Material for Lithium-ion Batteries at Room Temperature

Changjian Deng,[a] Miu Lun Lau,[a] Heather Barkholtz,[b] Haiping Xu,[b] Riley Parrish,[a] Meiyue Olivia Xu,[b] Tao Xu,[b] Yuzi Liu,[c] Hao Wang,[d] Justin G. Connell,[e] Kassiopeia A. Smith,[a] Hui Xiong*[a]

We report an amorphous boron nanorod anode material for lithium-ion batteries prepared through smelting non-toxic boron oxide in liquid lithium. Boron in theory can provide capacity as high as 3099 mAh g^{-1} by alloying with Li to form B_4Li_5. However, experimental studies of boron anode were rarely reported for room temperature lithium-ion batteries. Among the reported studies the electrochemical activity and cycling performance of bulk crystalline boron anode material are poor at room temperature. In this work, we utilized amorphous nanostructured one-dimensional (1D) boron material aiming at improving the electrochemical reactivity between boron and lithium ions at room temperature. The amorphous boron nanorod anode exhibited, at room temperature, a reversible capacity of 170 mAh g^{-1} at a current rate of 10 mA g^{-1} between 0.01 and 2 V. The anode also demonstrated good rate capability and cycling stability. Lithium storage mechanism was investigated by both sweep voltammetry measurements and galvanostatic intermittent titration technique (GITT). The sweep voltammetric analysis suggested that the contributions from lithium ions diffusion into boron as well as the capacitive process to the overall lithium charge storage are 57% and 43%, respectively. Results from GITT indicated that the discharge capacity at higher potentials (> ~ 0.2 V vs, Li/Li^+) could be ascribed to a capacitive process and at lower potentials (< ~0.2 V vs, Li/Li^+) to diffusion-controlled alloying reactions. Solid state nuclear magnetic resonance (NMR) measurement further confirmed that the capacity is from electrochemical reactions between lithium ions and the amorphous boron nanorod. This work provides new insights into designing nanostructured boron material for lithium-ion batteries.

Received 00th January 20xx,
Accepted 00th January 20xx

DOI: 10.1039/x0xx00000x

www.rsc.org/

Introduction

Rechargeable lithium-ion batteries (LIB) with high energy density, high power density and long cycle life are in urgent need for the surging markets in portable electronics and electrical vehicles (EVs). Graphite is commercially used as an anode material owing to its good rate capability, low irreversible capacity, and good cycle life. However, the relatively low theoretical specific capacity (372 mAh g^{-1}) of graphite has limited its further implementation in applications such as EVs. As a result, extensive research efforts have been carried out to improve anode performance by developing new materials such as alloy anode materials, which are expected to exhibit much higher theoretical specific capacities (two- to ten-fold increase) compared to commercial graphite anode[1].

Boron is an element of complexity. It exhibits the most varied polymorphisms of any of the elements: at least sixteen polymorphs have been reported to date[2] while the stable phase of boron is not yet established experimentally even at ambient conditions[3]. Boron's complexities arise from the fact that boron has only three valence electrons but sufficiently localized, which could shift between metallicity and insulating states by temperature, pressure and impurities[4-7]. The electron deficient nature of boron could facilitate inclusion of electrons while its common valence state (i.e., trivalent boron) could allow release the extra electrons. Hence, this property of boron can be utilized for charging/discharging.

Among the lithium-boron system, compounds such as B_3Li[8, 9], B_6Li_7[10], B_4Li_5[11-13] were reported, which in theory can provide 826, 2892, 3099 mAh g^{-1} in capacity, respectively. These compounds are generally composed of connected icosahedron B_{12} entities with Li residing between them.[9, 14] These systems are attractive for Li storage due to their high theoretical capacities and open structures for ion insertion. Although Li-B compound has been studied as anode material

[a] *Micron School of Materials Science and Engineering, Boise State University, Boise, ID 83725, USA. Email: clairexiong@boisestate.edu.*
[b] *Department of Chemistry and Biochemistry, Northern Illinois University, DeKalb, IL 60115, USA.*
[c] *Center for Nanoscale Materials, Argonne National Laboratory, Lemont, IL, 60439, USA.*
[d] *Chemical Science and Engineering Division, Argonne National Laboratory, Lemont, IL, 60439, USA*
[e] *Joint Center for Energy Storage Research, Argonne National Laboratory, Lemont, IL, 60439, USA*

Electronic Supplementary Information (ESI) available:Details of GITT techniques and the XPS survey scans of as-prepared and 1st cycles samples. See DOI: 10.1039/x0xx00000x

for thermal batteries since 1990s,[10, 15] the reports on boron anode materials for room temperature LIB are scarce. From the limited reports, the electrochemical reactivity as well as the cycling performance of bulk crystalline boron with lithium is poor at room temperature[16-20]. S. James investigated Li-B alloy in $LiClO_4$-propylene carbonate (PC) and stated that Li-B alloy is a mixture of pure lithium and a Li-B compound with a stoichiometry in the vicinity of "Li_7B_6" but no cycling performance of the electrode was reported[18]. Sanchez and Belin et al. determined Li-B alloy electrochemical properties in non-aqueous electrolytes[17]. The LiB compound was found to have some discharge capacity but its capacity decayed rapidly within only a few cycles[17]. Zhou et al. studied LiB compound[19] in the electrolyte of 1 M anhydrous $LiPF_6$ in a 1:1 mixture of ethylene carbonate (EC) and dimethyl carbonate (DMC), which exhibited a first discharge capacity of 226 mAh g^{-1} between 0 and 0.8 V versus Li/Li^+. The discharge capacity dropped to 149 mAh g^{-1} after 15 cycles. Recently, Ding *et al.* studied a new tetragonal boron (B_{50})[20] thin film with a thickness of 80 nm on a vanadium coated glass through a pulse laser deposition method. It was found that this thin film electrode exhibited only a capacity of 43 mAh g^{-1} in a nonaqueous electrolyte at room temperature[20]. Based on the first-principles calculations, the B_{50} is a metallic conductor and the very poor electrochemical activity at room temperature could be related to poor lithium ion diffusion (diffusion barrier is calculated as 2.59 eV) within the tetragonal B_{50} lattice. The charge storage capacity in the B_{50} film improves significantly at 85 ˚C, which is consistent with the first-principles simulations.

In this work, we developed amorphous nanostructured one-dimensional (1D) boron material aiming at improving lithium ion diffusion in boron at room temperature. The structure of amorphous boron is closely related to that of commonly found crystalline *β*-rhombohedral boron which consists of a complex three-dimensional array of B_{12} icosahedra subunits, but with disorder occurring at the linking between these subunits[21, 22]. Research has shown that there could be lower volume strain during cycling in amorphous structures than that in the corresponding crystalline one, which results in the promoted electrochemical stability of amorphous structures[23, 24] In addition, 1D nanostructured materials exhibit improved ion transport along the *z* axial direction, which leads to enhanced electrochemical performance[25-27]. Moreover, nanostructured materials can offer several advantages over their bulk counterparts: shorter diffusion length for both Li ion and electron transport; larger surface contact area enhancing kinetics at the electrode/electrolyte interface; better strain relaxation and volume accommodation, which lead to enhanced stability.

Herein, we tested amorphous boron nanorod anode for LIBs at room temperature, which exhibits a reversible capacity of 170 mAh g^{-1} at a 10 mA g^{-1} for 25 cycles. The unique amorphous nanostructure enhances the current reported capacity 43 mAh g^{-1} of crystalline boron anode by ~400% at the room temperature[20]. It also demonstrates a good rate capability and promising cycling performance, delivering up to 100 mAh g^{-1} reversible capacity after 500 cycles at 0.5 C rate (*nC* rate: discharge in *1/n* hours). Structural characterization by transition electron microscopy (TEM) and X-ray diffraction (XRD) reveals that the as-prepared boron nanorod electrode is amorphous. It is postulated through galvanostatic intermittent titration technique (GITT) measurement that the capacity at higher potential (> ~0.2 V vs. Li/Li^+) can be attributed to surface capacitive process and that at lower potential (< ~0.2 V vs. Li/Li^+) is due to solid state Li ions diffusion within B. To understand the contribution from each process, sweep voltammetry measurements were conducted and it was estimated that capacities resulting from diffusion control and from capacitive process are 57% and 43%, respectively. Solid state NMR further confirmed that lithium ions are actively involved in the electrochemical reaction with boron.

View Article Online
DOI: 10.1039/C7NR03017G

Experimental

Synthesis of amorphous boron nanorod

The amorphous boron nanorod materials were synthesized by our top down process reported previously.[28] 500 mg of B_2O_3 was dried at 110 °C under vacuum and then was thoroughly ground in the glove box. Subsequently, B_2O_3 powders were added into the molten Li with the molar ratio of B_2O_3:Li = 1:6 at 200 °C under sonication. Afterward, the temperature was increased to 250°C and maintained for 2 hours. After the reaction finished, the product was cooled down and taken out of the glove box. In order to obtain pure boron nanorod sample, the samples were first washed by methanol to remove unreacted lithium and then washed thoroughly with hot water, dilute potassium hydroxide solution, dilute hydrochloric acid solution and cold water to remove the Li, Li_2O, LiB_2, LiB_4 and B_2O_3 residues.

Characterizations

The XRD pattern was obtained by Rigaku Miniflex diffractometer with Cu Kα irradiation at λ = 1.5406 Å. The morphology and microstructures were examined by field emission scanning electron microscopy (FE-SEM, JEOL JSM-7500F field emission) and TEM (FEI Titan 80-300 ST). XPS was conducted by using Specs PHOIBOS 150 hemispherical energy analyzer using a monochromated Al Kα X-ray source. Survey spectra were collected using a pass energy of 40 eV, and spectra were referenced to the binding energy of graphite at 284.0 eV. XPS samples were loaded without air exposure through an Ar glovebox connected directly to the UHV system. Solid state ^7Li NMR measurement was performed with a Bruker Avance III spectrometer operating at a magnetic field strength of 7.04 T. A pulse delay of 10 s was used, and a total of 256 scans were acquired for each spectrum. The samples were spinning at 60 kHz at 283 K. Energy Dispersive X-Ray Spectroscopy (EDS) study of boron nanorods and the raw boron oxide powder was conducted

in a Tescan-Vega SEM equipped with an Oxford INCAx-act Analytical Standard EDS detector.

Electrochemical Measurement

Electrochemical characterization was conducted using a half-cell against a Li counter electrode. The boron electrodes were prepared by mixing of 70% boron active material, 10% graphite (Fisher Chemical), 10% super carbon C65 (Timcal America Inc.) and 10% sodium carboxymethylcellulose (CMC, Dow Chemical Company) and casting the slurry on copper current collector. After vacuum baked overnight at 70˚C, the electrode was punched into 1.5 cm dia. discs using Precision Disc Cutter (MTI) with a loading density of 0.6~0.8 mg cm^{-2}. Coin cells were prepared with boron electrode, Celgard 2325 separator, lithium (FMC) counter electrode in 1.2 M lithium hexafluorophosphate ($LiPF_6$) in ethyl carbonate (EC) and ethylmethyl carbonate (EMC) (3:7 w/w) in argon filled dry glove box (O_2 < 0.5 ppm). The coin cells were tested at 10 mA g^{-1} with the potential window from 0.01 to 2 V in an Arbin battery tester. A cell of three-electrode configuration was tested for CV with the potential window of 0.01 to 2 V at varying scan rates of 0.1 - 10 mV s^{-1}. CVs were conducted for at least three scans at each scan rate. GITT was conducted in a three-electrode cell with a potential window of 0.01 to 2 V at the rate of 10 mA g^{-1}. The cell was first cycled for 8 cycles and then discharged at 10 mA g^{-1} for a pulse of 30 min followed by a relaxation of 2 h to approach the steady state value. The process was repeated to the fully discharged state of 0.01 V.

Results and discussions

Our previous work[28] shows that nanoscale rod-like boron can be synthesized by simply smelting boron oxide powders in molten lithium under sonication. Hereby, we continue to utilize this method to synthesize boron nanorod and investigate the nanoscale electrochemical interactions between these born nanorods and lithium ions. The preparation of nano-rod boron materials can be found in our previous report[28]. In brief, the mixture of boron nanorod, Li, LiB_x, Li_2O and B_2O_3 were obtained after the reaction of B_2O_3 powders with molten Li under sonication. The mixture was then purified by alcohol, water, and diluted basic and acidic solutions in sequence to obtain pure amorphous boron nanorods.

The structure of boron material was examined by XRD, as shown in Fig. 1(a). Only a broad band with weak intensity was observed, which indicates the amorphous feature of the as-prepared sample. The crystallographic and morphological properties were determined by TEM. The 1D nano-rod structure with ~ 250 nm diameter was shown in Fig. 1(b). Moreover, the distribution of nanorod diameter is quite narrow, in agreement with the previous study.[26] Both the featureless image shown in Fig. 1(c) and the characteristic diffusive ring in the SAED pattern shown in Fig. 1(d) suggest that the as-prepared 1D boron nanorod is amorphous, which corroborates well with the XRD results.

View Article Online
DOI: 10.1039/C7NR03017G

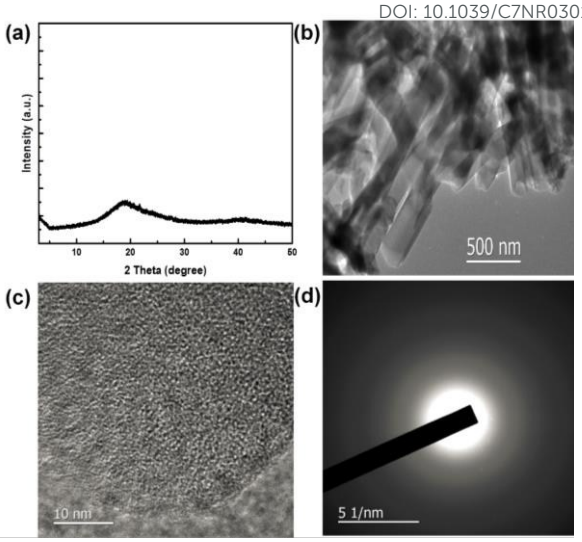

Fig. 1 (a) XRD pattern, (b) TEM image, (c) high resolution TEM image and (d) selected area electron diffraction (SAED) pattern of as prepared nano-rod boron materials.

The EDS study of the as-prepared sample and the raw boron oxide powder shows the nanorods are made of pure elemental boron (Supporting Information, Fig. S1). Fig. 2 (a) and (b) are as-prepared powders and cycled boron electrode, respectively. Both samples exhibit smooth surface with a uniform diameter of ~250 nm and a length ~ 1 um, which suggests that the 1D boron nanorod maintains its morphology after cycling. The preferential elongated nano-rod morphology instead of a nano-sphere one is due to the presence of sonication during the reaction of lithium with B_2O_3.[28, 29] The stream of ultrasonic propagation transfer momentum in the molten lithium solution, leading to a linear lithiation in B_2O_3 powders. Since the momentum distribution is not uniform in the lithium solution, the length of the nano-rods varies with momentum during lithiation.

The electrochemical performance of the amorphous boron nanorod anode was investigated using coin-type half cells with Li as the counter electrode. All of the coin cells were tested under room temperature. Fig. 3(a) showed the galvanostatic charge and discharge voltage profiles of the amorphous boron nanorod electrode at a current rate of 10 mA g^{-1} cycled between 0.01 and 2.0 V. The 1st cycle discharge and charge capacity are 419.10 and 205.16 mAh g^{-1}, respectively, corresponding to a Coulombic efficiency of 48.95%. The irreversible capacity loss might result from the formation of solid electrolyte interphase (SEI) between the electrode and the electrolyte, which commonly occurs in alloy anode[30]. After eight cycles, the electrode exhibits a reversible capacity ~ 170 mA g^{-1}, corresponding to a LiB_{15} compound, with a Coulombic efficiency of 97.7%. This reversible capacity is much higher than the previous report on a crystalline B_{50} thin film (44 mAh g^{-1}) at room temperature[20], which can be attributed to the improved lithium diffusion in 1D nanostructure and amorphous

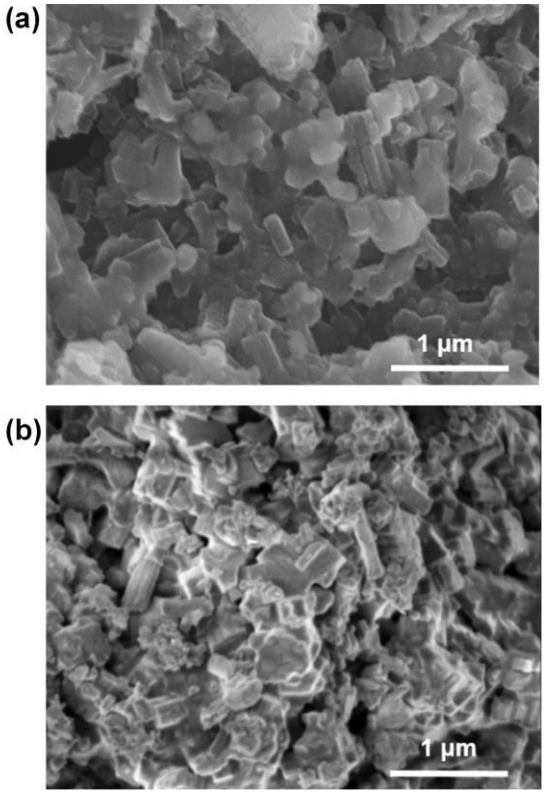

Fig. 2 FE-SEM images of (a) an as-prepared and (b) cycled nano-rod boron sample.

structure.[25] There are a few plateaus appeared in the charge/discharge curves at low voltages, indicating two phase regions of possible Li_xB alloy. The peaks shown in the differential capacity (dQ/dV) plots in Fig. 3(b) correspond to the plateaus observed in the charge/discharge curves (Fig. 3 (a)). During the first discharge, there are one irreversible peak at 1.0 V and three peaks at lower voltages (0.192 V, 0.106 V, and 0.069 V) clearly observable. During charge, three corresponding oxidation peaks are observed located at 0.237 V, 0.149 V and 0.107 V, respectively. The irreversible peak at 1 V is attributed to the side reaction between the electrode and the electrolyte and formation of SEI layer. The three redox peaks appeared here at lower voltages in dQ/dV plots are not shown in the B_{50} thin film reported previously[20], which explains why the amorphous boron nanorod electrode has much higher capacity due to enhanced electrochemical reactivity between lithium and the amorphous nanostructured boron. There are no additional peaks and no significant peak shift in all observed peaks in subsequent cycling, indicating the phase transitions are reversible.

Since one of the potential benefit of amorphous materials is the enhanced kinetics and electrochemical stability,[23, 24] we conducted experiments on the amorphous boron nanorod electrode for rate capability (Fig. 3c) and cycling performance (Fig. 3d) at a rate of 5 mA g^{-1} (0.5 C). The amorphous boron nanorod electrode exhibits great rate capability under different cycling rates varying from 10 to 1000 mA g^{-1} in Fig. 3(c). It delivered specific discharge

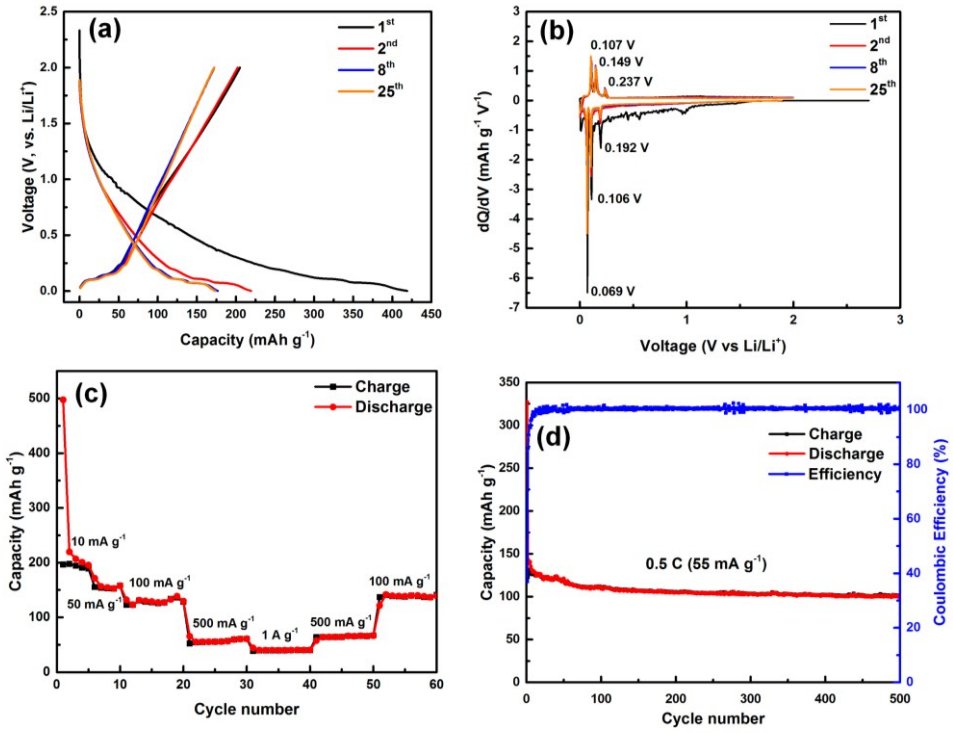

Fig. 3 Electrochemical characterization and electrode performance of the amorphous boron nanorod anode: (a) charge/discharge profile, (b) differential capacity versus voltage (dQ/dV) of the electrode cycled at 10 mA g^{-1}, (c) rate capability, and (d) cycling performance of the electrode with a current rate of 55 mA g^{-1}. All of above cycling are with the potential window 0.01~2 V vs. Li/Li^+ at room temperature.

capacities of 195.6, 157.8, 129.7, 60.9, and 40.3 mAh g^{-1} at current rates of 10, 50, 100, 500, and 1000 mA g^{-1}, respectively. The capacity moderately dropped with the increase of current density. At the highest current rate of 1 A g^{-1} the discharge capacity approached 40.6 mAh g^{-1}. When the current rates were ramped back to 500 and 100 mA g^{-1} after a variety of cycling rates its capacity return to ~64 and ~136 mAh g^{-1}, respectively, suggesting good capacity retention and rate capability. In the cycling performance study shown in Fig. 3(d), after 500 cycles, the electrode maintained a reversible capacity of 102 mAh g^{-1} with a capacity retention rate of 83.47%.

GITT measurement (Fig. 4(a)) was performed to understand the kinetic properties of the amorphous boron nanorod electrode, particularly Li diffusion coefficient during the electrochemical interaction between lithium and boron (the details of GITT analysis can be found in the Supporting Information). The log plot of the Li diffusivity as a function of voltage is shown in Fig. 4(b). It demonstrates that the diffusion associated with the sloping region (> ~0.2 V vs. Li/Li^+) is quite stable and is much faster than that of the plateau regions (< ~0.2 V). The diffusion coefficient dramatically drops when the voltage is below 0.2 V, where phase transitions occur as indicated by the dQ/dV plots shown in Fig. 3(b). The diffusion in the sloping region is about 2-order of magnitude larger than that of the plateau regions. This indicates that at the sloping region there are more accessible surface adsorptions sites for lithium ions diffusion. At the plateau regions (< ~0.2 V) where lithium and boron form alloys, the diffusion of lithium ions is poor as it has to overcome higher energy barriers to travel between B_{12} icosahedra. Since the capacity contributed from the sloping region is much larger than that from the plateau regions, the capacitive process plays a more significant role than that of the alloying reactions in lithium storage mechanism in this material. And the sluggish diffusion in alloying reactions might explain the lower capacity compared with the theoretical one.

In order to investigate the charge storage kinetics of the amorphous boron nanorod electrode, cyclic voltammograms (CVs) between 0.01 and 2 V with various scan rates of 0.1, 0.2, 0.5, 1.0 and 2.0 mV s^{-1} were performed (Fig. 4c). Low-potential region with the scan rate of 0.1 mV s^{-1} was highlighted in Fig. 4c inset, where three cathodic peaks at 0.16, 0.06, 0.01 V and three corresponding anodic peaks at 0.26, 0.22, 0.13 V can be resolved, in agreement with the dQ/dV plots shown in Fig. 3(b). The sweep voltammertry also provides insights in terms of diffusion and capacitive contribution of Li storage mechanism, which can be characterized by analyzing the data under various sweep rate according to[31]

$$i = av^b \quad (1)$$

Where measured current i obeys a power law relationship with scan rate. Both a and b in the equation are adjustable parameters. A b value of 1 indicates that the charge storage is controlled by a capacitor-like kinetics, which is one of the characteristic features of capacitive contribution.[32] A b=0.5 indicates that the charge storage process is limited by diffusion[33]. At potentials higher than ~ 0.2 V, the b-values are in the range of 0.73 – 0.75. At potentials smaller than ~ 0.2 V, the b-values are ~0.58, indicating that the charge storage mostly come from the Li ion alloying reactions. Since the

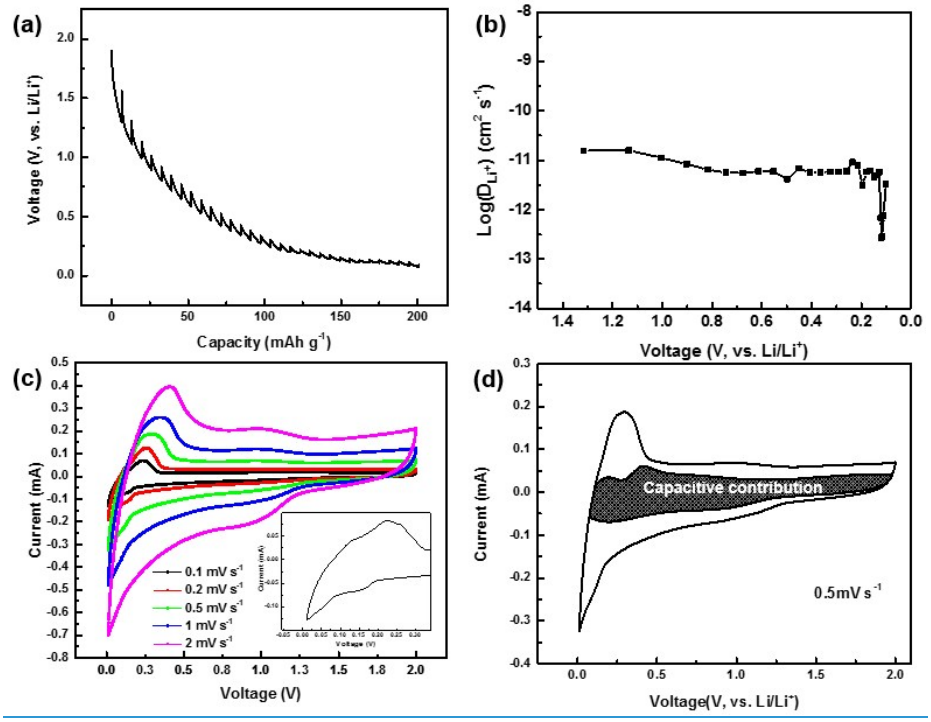

Fig. 4 (a) GITT profile. (b) Diffusivity as a function of states of charge. (c) Cyclic Voltammograms between 0.01 and 2 V with scan rate of 0.1, 0.2, 0.5, 1 and 2 mV s^{-1} (inset: low-potential region with the scan rate of 0.1 mV s^{-1}). (d) Capacitive contribution in the amorphous boron nanorod electrode at the scan rate of 0.5 mV s^{-1}.

capacitive contribution is involved in the process, we estimated the surface area normalized capacitance is larger than that of a typical double layer capacitator,10-50 μF cm^{-2},[34] indicating the lithium storage mechanism on the surface is dominated by pseudocapacitive contribution.

In addition, the diffusion and capacitive contribution to the current response at the fixed potential can be quantitatively examined by the following equation[32]:

$$i(V) = k_1 v + k_2 v^{1/2} \quad (2)$$

where the term $k_1 v$ and $k_2 v^{1/2}$ represent the contributions from surface capacitive and diffusion controlled process, respectively. Therefore, by determine both k_1 and k_2, we are able to quantitatively estimate the fraction of current contributed by capacitor-like process and those from the diffusion-limited process. The voltammetric response for the amorphous boron nanorod electrode at the slow scan rate of 0.5 mV s^{-1} in Fig. 4(d) demonstrates the contribution of a capacitor-like charge storage (shaded area) is quite significant, consistent with the electrochemical results discussed above. The diffusion-controlled contribution is largely occurring at the peak region at lower potentials, corresponding to the alloy reaction and is in agreement with the voltage profile (Fig. 3a) and GITT results (Fig. 4b). The capacitive process contributed ~ 43% of the total lithium charge storage, which is slightly smaller than that from the diffusion-controlled process related to Li alloying reactions (57%). This result indicates that increasing accessible surface sites for possible lithium ion adsorption through nanostructured boron compared to thin film boron could enhance the charge storage capacity.

To understand the chemical environment change of the amorphous boron nanorod electrode during cycling, *ex situ* XPS was performed with as-prepared and 1st discharged (lithiated) samples (Supporting Information, Fig. S4). Quantification of the surface speciation revealed that the atomic percentage of F increased with cycling, from 5% in the as-prepared sample to 22% in the 1st discharged sample, suggesting the growth of an SEI on the surface. Indeed, LiF is a common compound found in the SEI layer at alloy-type anodes.[30, 35] Although XPS analysis did not clearly show redox of the boron species, it is possible that surface reactions during sample transfer obscure lithiation in the bulk of the sample, which is not detected by the highly surface-sensitive XPS measurement. As a result, solid state ^{7}Li NMR was also performed to understand the chemical environment evolution in the bulk of the amorphous boron nanorod electrode upon cycling (Fig. 5). The ^{7}Li NMR spectra of a discharged (lithiated) and charged (delithiated) samples were normalized to the sample mass. One resonance was observed at around -1.0 ppm. The resonance of the charged sample suggests lithium retention from the previous cycling (potentially caused by the lithium ions trapping during the electrochemical process). It is also observed that the integrated area of the discharged spectrum is greater than

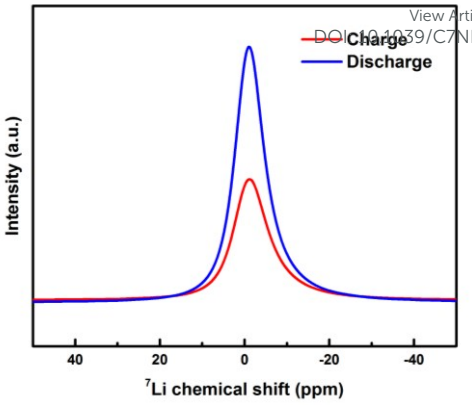

Fig. 5 Solid state ^{7}Li NMR spectroscopy of a charged and a discharged amorphous boron nanorod sample.

that of the charged one, suggesting lithium ions involvement in the electrochemical process. Additionally, the identical peak shape of these two spectra suggests that the chemical local environment in the charged or discharged samples remained the same.

Conclusions

Amorphous nanostructured 1D boron material was successfully prepared by the top-down process as anode for lithium ion batteries. At room temperature, it delivered 170 mAh g^{-1} reversible capacity at the rate of 10 mA g^{-1} between 0.01 and 2 V, which is four-fold larger than that from a previous study of crystalline boron thin film[20]. The electrode also exhibited promising rate capability, as well as cycling performance. It shows a reversible capacity of 100 mAh g^{-1} after 500 cycles at the rate of 0.5 C. GITT measurement indicated lithium diffusion due to surface adsorption at higher potential (> ~ 0.2 V vs. Li/Li$^+$) is significantly higher than that from alloying reactions at lower potentials (< ~0.2 V vs. Li/Li$^+$), which can be ascribed to the nanostructure effect. Sweep voltammetric analysis suggested that the contribution of pseudocapacitance to the lithium storage is larger than that from lithium diffusion in the alloying reactions. Our results indicate that the sluggish kinetics of lithium-boron alloying reactions impede the electrode from achieve its high theoretical capacity. Our work provides insights into materials design for new boron-related electrode materials such as borophene. We believe that tailoring the nanostructure as well as the surface chemistry of the boron electrode are critical to enhance its electrochemical reactivity at room temperature for lithium-ion batteries. Studies on the improvement of electrode kinetics are currently underway and could significantly improve the electrochemical performance of boron materials, therefore providing a new class of anode materials for lithium-ion batteries.

Notes

H. Xiong designed all experiments. T. Xu designed the synthesis of the material. C. Deng, M. Liu, and R. Parrish prepared the electrodes. C.Deng, M Liu, and R. Parrish conducted electrochemical measurements. C. Deng and H. Xiong analyzed the data. H. Barkohtlze, H. Xu, and M. Xu prepared the boron materials. Y. Liu and K. Smith conducted electron microscopic characterization. H. Wang collected and analyzed the solid ^{7}Li NMR data. J. Connell collected and analyzed the XPS data. All authors discussed the results and contributed to the manuscript preparation. C. Deng and H. Xiong wrote the manuscript.

Acknowledgements

H. Xiong gratefully acknowledges discussions with Dr. T. Rajh. T. Xu acknowledges the financial support from National Science Foundation (CBET-1150617). Use of the Center for Nanoscale Materials was supported by the U. S. Department of Energy, Office of Science, Office of Basic Energy Sciences, under Contract No. DE-AC02-06CH11357.

References

1 M. N. Obrovac and V. L. Chevrier, Chem Rev, 2014, 114, 11444-11502.
2 J. Donohue, Structures of the elements, John Wiley and Sons, Inc, United States, 1974.
3 M. Chase Tr, Journal, 1998, 9.
4 A. R. Oganov, J. H. Chen, C. Gatti, Y. Z. Ma, Y. M. Ma, C. W. Glass, Z. X. Liu, T. Yu, O. O. Kurakevych and V. L. Solozhenko, Nature, 2009, 457, 863-867.
5 T. Lundstrom, J Solid State Chem, 1997, 133, 88-92.
6 R. J. Nelmes, J. S. Loveday, D. R. Allan, J. M. Besson, G. Hamel, P. Grima and S. Hull, Phys Rev B, 1993, 47, 7668-7673.
7 E. Y. Zarechnaya, L. Dubrovinsky, N. Dubrovinskaia, Y. Filinchuk, D. Chernyshov, V. Dmitriev, N. Miyajima, A. El Goresy, H. F. Braun, S. Van Smaalen, I. Kantor, A. Kantor, V. Prakapenka, M. Hanfland, A. S. Mikhaylushkin, I. A. Abrikosov and S. I. Simak, Phys Rev Lett, 2009, 102.
8 G. Mair, H. G. von Schnering, M. Worle and R. Nesper, Z Anorg Allg Chem, 1999, 625, 1207-1211.
9 H. B. Borgstedt and C. Guminski, J Phase Equilib, 2003, 24, 572-574.
10 S. Dallek, D. W. Ernst and B. F. Larrick, J Electrochem Soc, 1979, 126, 866-870.
11 M. Worle and R. Nesper, Angew Chem Int Edit, 2000, 39, 2349-2353.
12 J. R. Letelier, Y. N. Chiu and F. E. Wang, J Less-Common Met, 1979, 67, 179-184.
13 F. E. Wang, Metall Trans A, 1979, 10, 343-348.
14 B. Albert, Eur J Inorg Chem, 2000, 1679-1685.
15 P. Sanchez, C. Belin, G. Crepy and A. Deguibert, J Mater Sci, 1992, 27, 240-246.
16 A. Netz, R. A. Huggins and W. Weppner, Ionics, 2001, 7, 433-439.
17 P. Sanchez, C. Belin, C. Crepy and A. Deguibert, J Appl Electrochem, 1989, 19, 421-428.
18 S. D. James, J Appl Electrochem, 1982, 12, 317-321.
19 D. B. Zhou, Z. J. Liu, X. K. Lv, G. S. Zhou and J. Yin, Electrochim Acta, 2006, 51, 5731-5737.
20 X. L. Ding, X. Lu, Z. Fu and H. Li, Electrochim Acta, 2013, 87, 230-235.
21 R. G. Delaplane, U. Dahlborg, W. S. Howells and T. Lundstrom, J Non-Cryst Solids, 1988, 106, 66-69.
22 R. G. Delaplane, U. Dahlborg, B. Graneli, P. Fischer and T. Lundstrom, J Non-Cryst Solids, 1988, 104, 249-252.
23 L. Y. Beaulieu, K. C. Hewitt, R. L. Turner, A. Bonakdarpour, A. A. Abdo, L. Christensen, K. W. Eberman, L. J. Krause and J. R. Dahn, J Electrochem Soc, 2003, 150, A149-A156.
24 T. D. Hatchard, M. N. Obrovac and J. R. Dahn, J Electrochem Soc, 2006, 153, A282-A287.
25 B. Wang, B. Luo, X. L. Li and L. J. Zhi, Mater Today, 2012, 15, 544-552.
26 H. Pang, X. Li, Q. Zhao, H. Xue, W.-Y. Lai, Z. Hu and W. Huang, Nano Energy, 2017, 35, 138-145.
27 B. Li, P. Gu, Y. Feng, G. Zhang, K. Huang, H. Xue and H. Pang, Adv Funct Mater, 2017, 27, n/a-n/a.
28 A. Chakrabarti, T. Xu, L. K. Paulson, K. J. Krise, J. A. Maguire and N. S. Hosmane, J Nanomater, 2010, DOI: Artn 589372 10.1155/2010/589372.
29 P. Marmottant and S. Hilgenfeldt, Nature, 2003, 423, 153-156.
30 E. Peled, D. Golodnitsky, C. Menachem and D. Bar-Tow, J Electrochem Soc, 1998, 145, 3482-3486.
31 H. Lindstrom, S. Sodergren, A. Solbrand, H. Rensmo, J. Hjelm, A. Hagfeldt and S. E. Lindquist, J Phys Chem B, 1997, 101, 7717-7722.
32 J. Wang, J. Polleux, J. Lim and B. Dunn, J Phys Chem C, 2007, 111, 14925-14931.
33 A. J. Bard and L. R. Faulkner, Electrochemical Methods: Fundamentals and Applications, John Wiley & Sons, New York, 1980.
34 B. E. Conway, V. Birss and J. Wojtowicz, J Power Sources, 1997, 66, 1-14.
35 A. M. Andersson and K. Edstrom, J Electrochem Soc, 2001, 148, A1100-A1109.